High-Pressure Clinical-Scale 87% Parahydrogen Generator

Jonathan R. Birchall, Aaron M. Coffey, Boyd M. Goodson, and Eduard Y. Chekmenev*

Cite This: https://dx.doi.org/10.1021/acs.analchem.0c03358

Read Online

ACCESS | Metrics & More | Article Recommendations | Supporting Information

ABSTRACT: We present an automated parahydrogen generator (Para-Sun) for clinical-scale applications in parahydrogen-induced polarization (PHIP) and signal amplification by reversible exchange (SABRE) at high pressures. The device employs a vacuum-pumped, Sunpower cryo-cooler (typically employed for cooling cellular network antennas) to achieve up to ~87% parahydrogen enrichment at a temperature as low as ~40 K and a maximum outlet pressure of ~490 PSI. The device reaches the target temperature set-point in under 1 h. It employs a FeO(OH) catalyst for the ortho- to para-state conversion. A mass-flow controller (MFC) facilitates the controlled flow of H_2 gas at a rate of 150 standard cubic centimeters per minute (sccm). This design bridges the gap between rudimentary 50% enrichment liquid-N_2 baths and far costlier, near-unity-enrichment configurations employing high-H_2 throughputs and <25 K temperatures. The design presented here should be of interest for those pursuing a wide variety of PHIP applications, including those involving the production of inhalable or injectable hyperpolarized contrast agents for biomedical imaging.
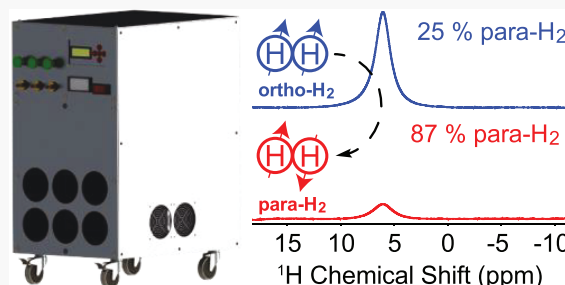
N MR hyperpolarization techniques are revolutionizing modern NMR spectroscopy and MRI imaging for a variety of applications by increasing the nuclear spin polarization P by several orders of magnitude, up to the order of unity.[1−5] As a result, it is possible to boost NMR/MRI signal by several orders of magnitude.[6] Biomedical applications are the main driver behind the development of hyperpolarized (HP) technologies,[7,8] and several HP techniques are now undergoing multiple clinical trials.[9,10] Parahydrogen (pH$_2$) induced polarization (PHIP) is an attractive hyperpolarization technique that employs pairwise pH$_2$ addition or reversible pH$_2$ exchange. Unlike many other hyperpolarization techniques, it offers the critical advantages of high speed and low cost with the key prerequisite of access to pH$_2$ gas.

At normal conditions (T = 298 K), H$_2$ gas is composed of 75% ortho- and 25% para-isomers based on the high-temperature statistical distribution of the molecules' nuclear spin-rotation states. To produce a substantial PHIP effect, a significant pH$_2$ enrichment over the normal 25% para-fraction must be achieved.[11] The para-state has lower energy compared to the ortho-state and therefore is strongly favored at temperatures below 25 K (>99% para-).[2,12] However, such low temperatures are challenging to achieve in practice, requiring bulky, specialized cryogenic equipment capable of several Watts of chilling capacity, resulting in a large (and potentially costly) footprint for pH$_2$ production.[13−17]

Conveniently, liquid N$_2$ (T = 77 K) can be employed to produce a 50% pH$_2$ fraction, which has shown to be a low-cost, facile route to enter the field of PHIP research.[18−20] However, this pH$_2$ fraction yields ~1/3 of the signal enhancement compared to the use of ≈100% pH$_2$. Yet in many PHIP

applications, the actual degree of polarization is critical (most notably biomedical applications), and a much higher pH$_2$ enrichment fraction is required.

Here, we describe the design and construction of a pH$_2$ generator based on a compact cryo-cooler employed industrially. This device is capable of reaching temperatures of 40−50 K and producing up to a 87% pH$_2$ fraction at up to 490 PSI. The commercially available Bruker pH$_2$ generator operates at up to 100 PSI in an automated manner and produces an >85% pH$_2$ fraction in an automated manner.[21] Compared to the Bruker device, our generator is capable of providing significantly higher pressures (up to 490 PSI), which has the practical advantages for hyperpolarization applications in the context of both hydrogenative[22] and non-hydrogenative PHIP (i.e., signal amplification by reversible exchange, SABRE).[23,24] Other than that, both devices have similarly a small footprint, low operational noise figure, low power consumption requirements (~600VA), fast cooldown time of ~1 h, and flow rates of up to 0.2 standard liter per minute (Bruker) and 0.15 standard liter per minute (our device). Other substantially higher-throughout generators have been commercialized,[15,16] e.g., the ARS-based generator by XeUS Technologies LTD, capable of producing over 4 standard liter per minute production rate of more than 98% pH$_2$. While

these devices provide both faster flow rates, high operating pressures (up to 50 atm), and better pH_2 fraction,[15] these are substantially more sophisticated installations with high noise figures, high power and heat loads requiring water cooling, and dedicated 220 VAC power lines. The reported here device bridges the gap between inexpensive and portable (but often rudimentary) liquid-N_2-based pH_2 generators, and high-performance (but significantly more expensive, bulky, and noisy) cryogenic generators. The described device is portable (with a small, low-noise footprint), is automated, and provides strong performance metrics quantified by the pH_2 fraction, operating pressure, and pH_2 throughput, all of which would likely be welcome by a variety of end users. Moreover, the estimated cost of the components is under $25,000.

■ MATERIALS AND METHODS

All components of the pH_2 generator are enclosed within a small-footprint aluminum frame (depth 27 in., width 18 in., height 34 in., Figure 1). The device (dubbed "ParaSun")
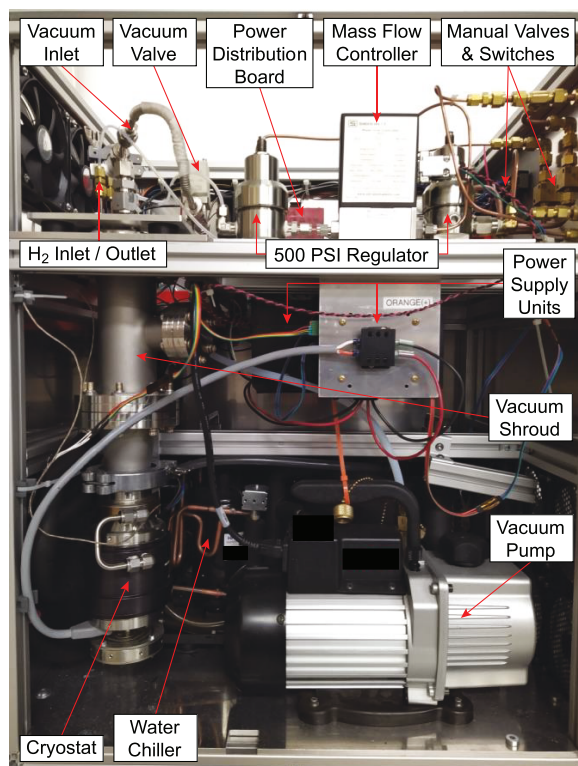

Figure 1. Annotated photograph of the interior or the pH_2 generator device and chassis, outlining the orientations and interfaces of the key components. The gas-handling manifold (upper section) is presented in greater detail in Figure 2.

operates at an H_2 inlet pressure of ~500 PSI as determined by a pair of single-stage inline regulators (KBP1J0A4A5A20000, Swagelok, Solon, OH) located at either side of a mass flow controller (MFC, C100L-DD-1-OV1-SV1-PV2-V1-S0-C0, Sierra Instruments, Monterey, CA) to prevent the backflow inside the manifold during venting. The typical H_2 flow rate during device operation is ~150 sccm using the installed MFC, faster flow rates are potentially possible (see discussion below).

Parahydrogen enrichment is performed using a 240 W vacuum-pumped liquid-N_2 cryo-cooler (CryoTel GT16-96, Sunpower Electronics, New Taipei City, Taiwan) capable of

achieving a catalyst chamber temperature of ~40 K in ~30 min. The cryo-cooler is a Sterling-cycle design and operates under a mass spring-damper system according to the specifications provided by the vendor. The lifetime of the cryo-cooler unit is estimated at 22 years under conditions of continuous use. The spin catalyst employed is paramagnetic hydrated iron(III) oxide ($Fe_2O_3 \cdot H_2O$, 371254, Sigma-Aldrich, St. Louis, MO). The catalyst is packed in a 3/16 in. diameter (0.128 in. inner diameter) cleaned copper tubing (McMaster Carr 5174K2) that forms a spiral around the cold-head (Figure 2 and the Supporting Information). Our initial attempt to use
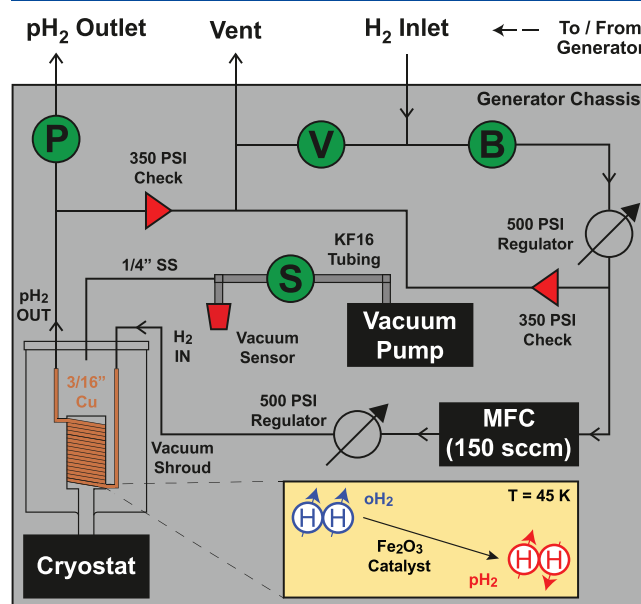

Figure 2. Schematic of the gas handling manifold employed on the pH_2 generator device for the purposes of H_2 gas flow and cryostat evacuation. Manual valves are indicated with green circles isolating the bulk H_2 inlet (B), atmospheric vent (V), and parahydrogen outlet (P). The vacuum solenoid valve is represented with a green circle (S). The 350−600 PSI check valves (set to ~600 PSI) at the MFC inlet and pH_2 outlet are portrayed with red triangles. Vacuum lines are stainless steel KF-16 (16 mm i.d. in size), reducing to 1/16 in. i.d. stainless steel (SS) when entering the vacuum shroud to minimize thermal losses inside the vacuum shroud. The H_2 pathway inside the vacuum shroud is adapted to 3/16 in. i.d. copper tubing to increase thermal coupling with the cold head of 5−10 g packed catalyst. All other manifold connections are 1/4 in. (internal) or 1/8 in. (external) copper tubing.

thinner 1/8 in. diameter copper tubing with substantially narrower cross-section (0.065 in. inner diameter) resulted in two issues: (i) packing of the catalyst along very long tubing was a practical challenge, and (ii) the resulting para-fraction was below the expected equilibrium value. A recirculating water chiller (EXC-800, Koolance, Auburn, WA), possessing 800 W of cooling power and a maximum flow rate of 11 L/min is used to draw generated heat away from the cryostat. The vacuum pump (VP4D, Miramar, FL) achieves an ultimate pressure of 10^{-2} Torr without cryo-pumping, as measured using a digital vacuum gauge (APG100-XLC Active Pirani NW16, Edwards, Burgess Hill, U.K.).

When operating the ParaSun generator, the required minimum pressure at the beginning of the cycle is $\sim 10^{-1}$ Torr at room temperature. Once the temperature reaches 100−110 K, the high vacuum-rated solenoid valve (XSA1-22

V-5G2, SMC Pneumatics, Yorba Linda, CA) is closed and the pump is turned off (Figure 2) for the remainder of the production cycle to isolate the gas-handling manifold from the vacuum chamber. Below this temperature, the cryo-cooler enables condensation of volatile molecules leading to cryogenic pressure reduction, normally, the vacuum gauged is zeroed (i.e., below 5.75×10^{-6} Torr as seen on the vacuum sensor). A pair of 350–600 PSI one-way check-valves (B-4CPA2-350, Swagelok, Solon, OH) set to ~600 PSI are situated before the MFC and at the pH_2 gas outlet, both leading to the vent exit path. This ensures a sufficient pressure is maintained inside the cryostat and there is no overpressurizing backflow of gas into the device (which may otherwise cause structural damage). A series of manual valves situated on the external front face of the pH_2 generator chassis are used to control the flow of gas into and out of the device.

Electric power is provided to each component via distribution boards. The MFC, vacuum solenoid valve, and heating element are actuated through a series of heat-sunk solid state relays (SSR-25DA), and DC output modules (70G-ODC5, Grayhill, La Grange, IL) are operated using 24 VDC provided by a separate power supply unit (S8VK-G03024, OMRON Corporation, Kyoto, Japan). Cooling of the chassis is provided by a series of external fans (A12025-12CB-3BN-F1, CoolerMaster, New Taipei City, Taiwan), each rated to 12 V and powered by a single-output AC-DC power supply (VDRS-100-12, CUI Inc., Tualatin, OR). The cryostat is actuated by a 48 VDC power supply unit (S8VK-G48048, OMRON Corporation, Kyoto, Japan) and a step-down DC current regulator module (GT 48 V RTD, Sunpower Electronics, New Taipei City, Taiwan), see the Supporting Information for details. An additional OMRON power supply unit (S8VK-G01505, OMRON Corporation, Kyoto, Japan) provides a 5 VDC supply needed to power an Arduino automation microcontroller (not utilized in the current design but potentially compatible as previously shown in SEOP hyper-polarizers[25]). Each of these six components can be independently actuated on and off via a switch located on the front panel of the pH_2 generator device (although these components can be toggled automatically using an afore-mentioned Arduino microcontroller if desired and implemented).

Before pH_2 gas generation commences, it is necessary to flush residual contaminants such as oxygen from the manifold (shown in greater detail in Figure 2) for ~10 min using source H_2. This practice helps to minimize the risk of residual contaminant gases freezing inside the catalyst chamber and causing a blockage and also to ensure MFC operation feedback. When evacuating the vacuum shroud of the cryo-cooler, an initial vacuum level of ~10^{-1} Torr is obtained before commencing cooling via the water chiller and cryo-cooler. After initialization, the cryo-cooler will begin cooling the catalyst chamber at the minimum operating power of 70 W. The cryostat temperature can be monitored and controlled remotely via the vertically inserted thermocouple, which is externally connected to a USB serial terminal application such as CoolTerm. By varying the power that is supplied to the cryo-cooler, a reduction in temperature (and subsequent enrichment in pH_2 fraction) can be achieved. Once the temperature has been stabilized at the 40–50 K range, the pH_2 generator is ready for use. In order to safely return the cryostat catalyst chamber to room temperature (i.e., after desired experimentation has been concluded), an ~5 W heating

element is employed to raise the catalyst chamber temperature above 77 K, after which the cryo-cooler catalyst chamber, water chiller, and heater can all be switched off to allow the system to safely return to ambient temperature. Finally, power to the device can be switched off after closing the H_2 inlet valve, pH_2 outlet valve, and MFC. A complete synopsis of the experimental procedure for producing pH_2 can be found in the Supporting Information.

■ RESULTS AND DISCUSSION

Using this operational procedure, a sample of parahydrogen-enriched H_2 gas was collected into a high-throughput 5 mm NMR tube after 1 h of operation at a cryo-cooler temperature of ~40 K. ^1H NMR spectroscopy (700 MHz Bruker Avance NMR spectrometer for Figure 3a,b; 400 MHz Varian NMR
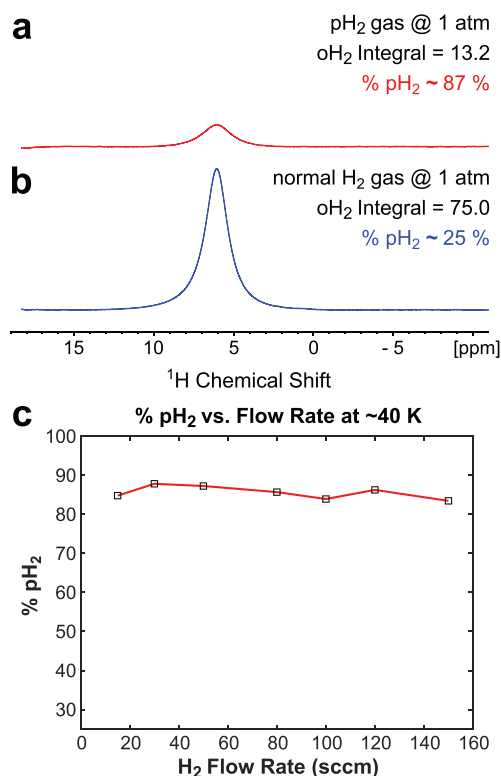

Figure 3. Orthohydrogen (oH_2) ^1H NMR spectra of (a) 87%-enriched pH_2 gas collected from the generator outlet after 1 h of cryostat operation at ~40 K (as sensed by a thermocouple, note that 87%), red; (b) source H_2 gas (75% triplet oH_2, 25% singlet pH_2), blue. Both spectra were recorded at 700 MHz using identical acquisition parameters (see text).

spectrometer for Figure 3c) was performed to analyze the residual signal from orthohydrogen (oH_2); note that pH_2 is NMR invisible and oH_2 exhibits broad lines due to efficient T_1 relaxation in the gas phase.[11] An oH_2 NMR spectrum of this pH_2-enriched sample was compared to a corresponding NMR spectrum of normal H_2 gas containing 75% oH_2 and 25% pH_2. Each spectrum was acquired using a spectral width of 21 kHz, 512 scans, 92 ms repetition time, 49 ms acquisition time, and $t_{90°}$ (7.5 μs using 700 MHz NMR spectrometer and 10 μs using Varian NMR spectrometer). Spectra were processed with 10 Hz line broadening. The results from this comparison are shown in Figure 3.

The spectral intensity arising from the NMR-visible oH_2 triplet state (normalized to an integral value of 75.0 corresponding to the 75% population of H_2 nuclear spins in the oH_2 triplet state at thermal equilibrium) is reduced by more than a factor of 5 following pH_2-enrichment at ~40 K (sensor reading). The reduction in oH_2 NMR spectral intensity corresponds to an increase in population of the NMR-invisible pH_2 singlet state. The normalized integral of 13.2 translates to an oH_2 triplet population of ~13 $\pm$ 2%, inversely indicating a pH_2 singlet fraction of 87 $\pm$ 2%. This ability to continuously produce pH_2 at this high level of enrichment has several practical benefits. First, it enables studies that continuously consume pH_2 at flow rates of <150 sccm. We note that the flow rates of 100 sccm and below result in an ~40 K equilibrium temperature, whereas a higher flow rate (e.g., 150 sccm corresponding to 42 K in Figure 3c) leads to the an overall higher heat load (due to incoming H_2 gas) and a higher equilibrium temperature resulting in the overall slightly lower pH_2 fraction, Figure 3c; however, we find the device performance at 150 sccm and below very satisfactory. Moreover, the minor discrepancy between the observed % pH_2 and the theoretical value (Table S1) and the observed small oscillation in the flow rate dependence data (Figure 3c) are due to a series of compounding factors: (i) differential relaxation of pH_2 gas in NMR tubes (due to collision with wall residual atmospheric O_2) during the time between sample collection and NMR acquisition (~10 min), (ii) small differences in the sample filling, and (iii) thermocouple temperature reading. The oscillation and the discrepancies can be potentially avoided using benchtop NMR spectroscopy of a high-pressure continuous-flow setup, work in progress in our laboratory. Despite these minor deficiencies, we find the performance of the ParaSun generator very robust and satisfactory in a broad range of flow rates (Figure 3c).

The pH_2 production using this generator enabled PHIP studies in our laboratory over several years of research including those when pH_2 is bubbled through solutions residing in 5 mm NMR tubes (under high pH_2 pressure of up to 100 PSI overpressure)[26−33] and also for clinical scale production of HP hydrocarbon gases;[34,35] sample pressures up to 490 PSI are possible with this device. Second, the use of high pressure allows for preparation of premixed binary and ternary mixtures, when pH_2 is added on "top" of other gases (e.g., propylene), which have relatively low equilibrium pressure. Moreover, substantial overpressure with pH_2 allows performing hydrogenation reactions of otherwise volatile compounds: e.g., hydrogenation of diethyl ether at 75 °C (normal bp 35 °C).[36] Lastly, the use of high-pressure production allows for filling of aluminum tanks with pH_2, where the singlet state can be preserved for weeks.[16]

Although the current design can enable flow rates substantially greater than 150 sccm, the heat load of warm H_2 gas entering the catalyst spiral results in a higher temperature of the coldhead and consequently a lower para-fraction (Table S1). For example, the 150 sccm flow rate in Figure 3c results in an ~42 K equilibrium temperature of the cold head, whereas the flow rate of 100 sccm and below resulted in the corresponding temperature of ~40 K. This device was produced in two replica copies now installed at Wayne State University (Detroit, MI) and Southern Illinois University Carbondale (Carbondale, IL).

CONCLUSIONS

The ParaSun parahydrogen generator design presented here demonstrates the ability to produce highly enriched pH_2 at high outlet pressures of up to 490 PSI. The employed design achieves a catalyst chamber temperature of ~40 K, resulting in apparent ~87% pH_2 enrichment as confirmed by NMR spectroscopy approximately 10 min after sample collection. The use of 87% pH_2 improves PHIP NMR signals by ~2.4-fold compared to those obtained in liquid N_2 setups. Of note, the additional PHIP signal improvement of using >99% pH_2 generator over 87% pH_2 enrichment is a factor of 1.2. A 150 sccm mass flow controller (MFC) is employed to ensure consistent throughput of H_2 gas from an inlet pressure of 500 PSI. This pH_2 production process can be utilized in both hydrogenative and non-hydrogenative PHIP techniques to efficiently hyperpolarize compounds relevant to a wide range of studies varying from catalysis, to chemical analysis, to biomedicine. Indeed, the information presented here has exciting potential for application in clinical-scale hyperpolarization of a number of liquid and gaseous contrast agents in biomedical imaging utilizing both PHIP and SABRE methodologies.

ASSOCIATED CONTENT

ⓢ Supporting Information

The Supporting Information is available free of charge at https://pubs.acs.org/doi/10.1021/acs.analchem.0c03358.

> Additional annotated schematics, 3D renderings and photographs describing the design of the pH_2 generator device, and instructional manual for configuration and daily operation (PDF)

AUTHOR INFORMATION

Corresponding Author

Eduard Y. Chekmenev − *Department of Chemistry, Integrative Biosciences (Ibio), Wayne State University, Karmanos Cancer Institute (KCI), Detroit, Michigan 48202, United States; Russian Academy of Sciences, Moscow 119991, Russia;* ⓞ orcid.org/0000-0002-8745-8801; Email: chekmenevlab@gmail.com

Authors

Jonathan R. Birchall − *Department of Chemistry, Integrative Biosciences (Ibio), Wayne State University, Karmanos Cancer Institute (KCI), Detroit, Michigan 48202, United States;* ⓞ orcid.org/0000-0003-3920-4038

Aaron M. Coffey − *Department of Radiology, Vanderbilt University Institute of Imaging Science (VUIIS), Nashville, Tennessee 37232, United States*

Boyd M. Goodson − *Department of Chemistry and Biochemistry and Materials Technology Center, Southern Illinois University, Carbondale, Illinois 62901, United States;* ⓞ orcid.org/0000-0001-6079-5077

Complete contact information is available at:
https://pubs.acs.org/10.1021/acs.analchem.0c03358

Notes

The authors declare the following competing financial interest(s): B.M.G. and E.Y.C. declare a stake of ownership in XeUS Technologies Ltd. (Cyprus).

■ REFERENCES

(1) Nikolaou, P.; Coffey, A. M.; Walkup, L. L.; Gust, B. M.; Whiting, N.; Newton, H.; Barcus, S.; Muradyan, I.; Dabaghyan, M.; Moroz, G. D.; Rosen, M.; Patz, S.; Barlow, M. J.; Chekmenev, E. Y.; Goodson, B. M. *Proc. Natl. Acad. Sci. U. S. A.* **2013**, *110* (35), 14150−14155.

(2) Goodson, B. M.; Whiting, N.; Coffey, A. M.; Nikolaou, P.; Shi, F.; Gust, B. M.; Gemeinhardt, M. E.; Shchepin, R. V.; Skinner, J. G.; Birchall, J. R.; Barlow, M. J.; Chekmenev, E. Y. *Emagres* **2015**, *4* (4), 797−810.

(3) Nikolaou, P.; Goodson, B. M.; Chekmenev, E. Y. *Chem. - Eur. J.* **2015**, *21* (8), 3156−3166.

(4) Ardenkjaer-Larsen, J. H.; Fridlund, B.; Gram, A.; Hansson, G.; Hansson, L.; Lerche, M. H.; Servin, R.; Thaning, M.; Golman, K. *Proc. Natl. Acad. Sci. U. S. A.* **2003**, *100* (18), 10158−10163.

(5) Fekete, M.; Ahwal, F.; Duckett, S. B. *J. Phys. Chem. B* **2020**, *124* (22), 4573−4580.

(6) Golman, K.; Axelsson, O.; Johannesson, H.; Mansson, S.; Olofsson, C.; Petersson, J. S. *Magn. Reson. Med.* **2001**, *46* (1), 1−5.

(7) Kurhanewicz, J.; Vigneron, D. B.; Brindle, K.; Chekmenev, E. Y.; Comment, A.; Cunningham, C. H.; DeBerardinis, R. J.; Green, G. G.; Leach, M. O.; Rajan, S. S.; Rizi, R. R.; Ross, B. D.; Warren, W. S.; Malloy, C. R. *Neoplasia* **2011**, *13* (2), 81−97.

(8) Kurhanewicz, J.; Vigneron, D. B.; Ardenkjaer-Larsen, J. H.; Bankson, J. A.; Brindle, K.; Cunningham, C. H.; Gallagher, F. A.; Keshari, K. R.; Kjaer, A.; Laustsen, C.; Mankoff, D. A.; Merritt, M. E.; Nelson, S. J.; Pauly, J. M.; Lee, P.; Ronen, S.; Tyler, D. J.; Rajan, S. S.; Spielman, D. M.; Wald, L.; Zhang, X.; Malloy, C. R.; Rizi, R. *Neoplasia* **2019**, *21* (1), 1−16.

(9) Nelson, S. J.; Kurhanewicz, J.; Vigneron, D. B.; Larson, P. E. Z.; Harzstark, A. L.; Ferrone, M.; van Criekinge, M.; Chang, J. W.; Bok, R.; Park, I.; Reed, G.; Carvajal, L.; Small, E. J.; Munster, P.; Weinberg, V. K.; Ardenkjaer-Larsen, J. H.; Chen, A. P.; Hurd, R. E.; Odegardstuen, L. I.; Robb, F. J.; Tropp, J.; Murray, J. A. *Sci. Transl. Med.* **2013**, *5* (198), 198ra108.

(10) Driehuys, B.; Martinez-Jimenez, S.; Cleveland, Z. I.; Metz, G. M.; Beaver, D. M.; Nouls, J. C.; Kaushik, S. S.; Firszt, R.; Willis, C.; Kelly, K. T.; Wolber, J.; Kraft, M.; McAdams, H. P. *Radiology* **2012**, *262* (1), 279−289.

(11) Hövener, J.-B.; Pravdivtsev, A. N.; Kidd, B.; Bowers, C. R.; Glöggler, S.; Kovtunov, K. V.; Plaumann, M.; Katz-Brull, R.; Buckenmaier, K.; Jerschow, A.; Reineri, F.; Theis, T.; Shchepin, R. V.; Wagner, S.; Bhattacharya, P.; Zacharias, N. M.; Chekmenev, E. Y. *Angew. Chem., Int. Ed.* **2018**, *57* (35), 11140−11162.

(12) Farkas, A. *Orthohydrogen, Parahydrogen, and Heavy Hydrogen*; Cambridge University Press: Cambridge, U.K., 1935.

(13) Hövener, J.-B.; Chekmenev, E. Y.; Harris, K. C.; Perman, W.; Robertson, L.; Ross, B. D.; Bhattacharya, P. *MAGMA* **2009**, *22*, 111−121.

(14) Hövener, J.-B.; Chekmenev, E. Y.; Harris, K. C.; Perman, W.; Tran, T.; Ross, B. D.; Bhattacharya, P. *MAGMA* **2009**, *22*, 123−134.

(15) Hövener, J.-B.; Baer, S.; Leupold, J.; Jenne, K.; Leibfritz, D.; Hennig, J.; Duckett, S. B.; von Elverfeldt, D. *NMR Biomed.* **2013**, *26* (2), 124−131.

(16) Feng, B.; Coffey, A. M.; Colon, R. D.; Chekmenev, E. Y.; Waddell, K. W. *J. Magn. Reson.* **2012**, *214*, 258−262.

(17) Kadlecek, S.; Vahdat, V.; Nakayama, T.; Ng, D.; Emami, K.; Rizi, R. *NMR Biomed.* **2011**, *24* (8), 933−942.

(18) Gamliel, A.; Allouche-Arnon, H.; Nalbandian, R.; Barzilay, C. M.; Gomori, J. M.; Katz-Brull, R. *Appl. Magn. Reson.* **2010**, *39* (4), 329−345.

(19) Plaumann, M.; Bommerich, U.; Trantzschel, T.; Lego, D.; Dillenberger, S.; Sauer, G.; Bargon, J.; Buntkowsky, G.; Bernarding, J. *Chem. - Eur. J.* **2013**, *19* (20), 6334−6339.

(20) Buljubasich, L.; Prina, I.; Franzoni, M. B.; Münnemann, K.; Spiess, H. W.; Acosta, R. H. *J. Magn. Reson.* **2013**, *230*, 155−159.

(21) Buljubasich, L.; Franzoni, M. B.; Spiess, H. W.; Munnemann, K. *J. Magn. Reson.* **2012**, *219*, 33−40.

(22) Shchepin, R. V.; Barskiy, D. A.; Coffey, A. M.; Manzanera Esteve, I. V.; Chekmenev, E. Y. *Angew. Chem., Int. Ed.* **2016**, *55* (20), 6071−6074.

(23) Truong, M. L.; Theis, T.; Coffey, A. M.; Shchepin, R. V.; Waddell, K. W.; Shi, F.; Goodson, B. M.; Warren, W. S.; Chekmenev, E. Y. *J. Phys. Chem. C* **2015**, *119* (16), 8786−8797.

(24) Adams, R. W.; Aguilar, J. A.; Atkinson, K. D.; Cowley, M. J.; Elliott, P. I. P.; Duckett, S. B.; Green, G. G. R.; Khazal, I. G.; Lopez-Serrano, J.; Williamson, D. C. *Science* **2009**, *323* (5922), 1708−1711.

(25) Nikolaou, P.; Coffey, A. M.; Walkup, L. L.; Gust, B. M.; Whiting, N. R.; Newton, H.; Muradyan, I.; Dabaghyan, M.; Ranta, K.; Moroz, G.; Patz, S.; Rosen, M. S.; Barlow, M. J.; Chekmenev, E. Y.; Goodson, B. M. *Magn. Reson. Imaging* **2014**, *32* (5), 541−550.

(26) Shchepin, R. V.; Birchall, J. R.; Chukanov, N. V.; Kovtunov, K. V.; Koptyug, I. V.; Theis, T.; Warren, W. S.; Gelovani, J. G.; Goodson, B. M.; Shokouhi, S.; Rosen, M. S.; Yen, Y.-F.; Pham, W.; Chekmenev, E. Y. *Chem. - Eur. J.* **2019**, *25*, 8829−8836.

(27) Theis, T.; Ariyasingha, N. M.; Shchepin, R. V.; Lindale, J. R.; Warren, W. S.; Chekmenev, E. Y. *J. Phys. Chem. Lett.* **2018**, *9*, 6136−6142.

(28) Ariyasingha, N. M.; Lindale, J. R.; Eriksson, S. L.; Clark, G. P.; Theis, T.; Shchepin, R. V.; Chukanov, N. V.; Kovtunov, K. V.; Koptyug, I. V.; Warren, W. S.; Chekmenev, E. Y. *J. Phys. Chem. Lett.* **2019**, *10*, 4229−4236.

(29) Gemeinhardt, M. E.; Limbach, M. N.; Gebhardt, T. R.; Eriksson, C. W.; Eriksson, S. L.; Lindale, J. R.; Goodson, E. A.; Warren, W. S.; Chekmenev, E. Y.; Goodson, B. M. *Angew. Chem., Int. Ed.* **2020**, *59* (1), 418−423.

(30) Kidd, B. E.; Gesiorski, J. L.; Gemeinhardt, M. E.; Shchepin, R. V.; Kovtunov, K. V.; Koptyug, I. V.; Chekmenev, E. Y.; Goodson, B. M. *J. Phys. Chem. C* **2018**, *122* (29), 16848−16852.

(31) Kidd, B.; Mashni, J.; Limbach, M.; Shi, F.; Chekmenev, E. Y.; Hou, Y.; Goodson, B. M. *Chem. - Eur. J.* **2018**, *24* (42), 10641−10645.

(32) Chukanov, N. V.; Salnikov, O. G.; Shchepin, R. V.; Svyatova, A.; Kovtunov, K. V.; Koptyug, I. V.; Chekmenev, E. Y. *J. Phys. Chem. C* **2018**, *122* (40), 23002−23010.

(33) Salnikov, O. G.; Chukanov, N. V.; Shchepin, R. V.; Manzanera Esteve, I. V.; Kovtunov, K. V.; Koptyug, I. V.; Chekmenev, E. Y. *J. Phys. Chem. C* **2019**, *123* (20), 12827−12840.

(34) Ariyasingha, N. M.; Salnikov, O. G.; Kovtunov, K. V.; Kovtunova, L. M.; Bukhtiyarov, V. I.; Goodson, B. M.; Rosen, M. S.; Koptyug, I. V.; Gelovani, J. G.; Chekmenev, E. Y. *J. Phys. Chem. C* **2019**, *128* (18), 11734−11744.

(35) Salnikov, O. G.; Nikolaou, P.; Ariyasingha, N. M.; Kovtunov, K. V.; Koptyug, I. V.; Chekmenev, E. Y. *Anal. Chem.* **2019**, *91* (7), 4741−4746.

(36) Ariyasingha, N. M.; Joalland, B.; Younes, H. R.; Salnikov, O. G.; Chukanov, N. V.; Kovtunov, K. V.; Kovtunova, L. M.; Bukhtiyarov, V. I.; Koptyug, I. V.; Gelovani, J. G.; Chekmenev, E. Y. *Chem. - Eur. J.* **2020**, *26*, 13621−13626.